



# Large Eddy Simulation of Pulsed Blowing in a Supersonic Compressor Cascade

Q. Meng, S. Chen<sup>†</sup>, S. Ding, H. Liu and S. Wang

*Harbin Institute of Technology, Harbin, Heilongjiang, 150001, China*

<sup>†</sup>Corresponding Author Email: [cswemail@hit.edu.cn](mailto:cswemail@hit.edu.cn)

(Received March 18, 2019; accepted July 13, 2019)

## ABSTRACT

Large Eddy Simulation (LES) of a two dimensional supersonic compressor cascade is performed in the current study. It is found that the Shock Wave Boundary Layer Interaction causes a large scale of total pressure losses and presents strong fluctuation features. Thus the pulsed and steady excitation jets are applied to suppress the flow separations and to reduce the total pressure losses. Several impacting parameters, such as jet axial location, jet hole width, jet angle to the local blade surface and jet mass flowrate are chosen based on the primary analysis by the calculations by the Reynolds Averaged Navier-Stokes equations. In addition, based on the results of frequency spectrum and POD analysis, the excitation jet frequency is chosen for the pulsed excitation jet scheme. It is concluded that the pulsed excitation jet scheme achieves a 9.8% reduction of total pressure loss in comparison to the steady excitation jet scheme under the same time-averaged excitation jet mass flow rate. The excitation jets affect both the flow field near the jet hole on the suction surface and the flow field on the pressure surface via the management of the reflection shock wave. In addition, the excitation frequency dominates not only the time-averaged flow field, but also the second and third modes which stand for the unsteady structures in the flow field under the POD analysis. The first mode contains most energy in the flow field and the energy percentage decreases dramatically with the increase of the mode number. In comparison to the steady excitation jet scheme, the pulsed excitation jet scheme gathers more energy to the low orders of the modes, especially the first four modes. With the mixing effect and high dissipation rate of the high-frequency signals, the high-frequency signals shrink in the wake and the flow field builds up more uniformity.

**Keywords:** Large eddy simulation; Pulsed blowing; Supersonic compressor; Proper orthogonal decomposition; Loss reduction

## 1. INTRODUCTION

The trend of reducing the compressor size and weight by means of reducing the number of stages results in a higher pressure ratio per stage. Shock waves can provide considerable pressure rise and have drawn researchers' attentions. Appropriate management of shock wave structure seems particularly essential since shock waves may introduce substantial aerodynamic losses. Although the flow phenomena can be highly three dimensional in nature in the supersonic compressor cascades, systematic analysis of the flow field under two dimensional cascade is still an important method to investigate the mechanism of mitigating aerodynamic losses and preserving advantages of the shock wave compression effect (Venturelli *et al.*, 2016).

The supersonic compressor cascades are mainly subjected to two sources (Bölcs *et al.*, 1986) of

aerodynamic losses: the entropy rise across the shock wave and the losses originated in the shock wave boundary layer interaction (SWBLI) process. Weakening the shock wave intensity by means of reducing the Mach number ahead of the shock wave or moving the normal shock wave to an oblique shock wave can moderate the entropy rise and has been widely studied in former studies (Liu *et al.*, 2017; Biollo *et al.*, 2013; Calvert *et al.*, 1994). Thus the current study focuses on the reduction of losses originated in the SWBLI. The boundary layer conditions were pointed out to be an important impacting factor in the behavior of SWBLI (Liepmann *et al.*, 1951; Priebe *et al.*, 2009). For the laminar boundary layer, a separation bubble appears near the shock wave reflection point. While for the turbulent boundary layer, the shock wave may disturb the boundary layer with or without separation. Quite different flow features would be observed accordingly. Besides, the Mach number before the shock wave was also reported to be an

essential impacting factor on the SWBLI structures (Horstman *et al.*, 1977). Pearcey *et al.* (1959) concluded that a Mach number of 1.27 or a pressure rise ratio of 1.4 over the shock wave is a criterion for determining whether separation occurs in the boundary layer with the study over an airfoil. However, in Chauvin *et al.*'s (1969) and Griepentrog's (1972) studies, a static pressure rise ratio of 1.5 could be more appropriate for determining the occurrence of separation in the boundary layer if taking the difference of airfoils and compressor profiles into consideration.

Another widely reported character in the supersonic compressor cascade flow field with the SWBLI structure turns out to be the strong unsteady features. If identify the unsteady features with the standard of frequency, the high frequency features are believed to be relative to the inflow turbulence intensity (Priebe *et al.*, 2009; Kuacutė *et al.*, 1998). Currently, the low frequency signals are not clearly related to particular flow field parameters and they occupy most of the turbulent energy (Pasquariello *et al.*, 2017). Some investigations (Priebe *et al.*, 2009; Humble *et al.*, 2009; Priebe *et al.*, 2012; Vanstone *et al.*, 2016) pointed out the importance of the coherent structure and the boundary layer conditions upstream of the shock wave foot. On the contrary, the boundary layer conditions downstream of the shock wave was supposed to be the key factor in the studies of Priebe *et al.* (2012) and Clemens *et al.* (2014). The flow field unsteadiness is a complicated issue and Proper Orthogonal Decomposition (POD) method is employed in the current study. POD was first introduced in the analysis of turbulent flows by Lumley *et al.* (1967). In Soni *et al.*'s (2017) study, the reconstructed flow fields under different POD modes were pointed out to correspond to different features in the coherent structures. Currently, few researches employ POD analysis in turbomachinery. Cizmas *et al.* (2003) applied POD analysis to the study of turbine rotor-stator interaction and validated a reduced order model for the problem.

Flow control methods have a great potential to break the fundamental barriers of traditional supersonic compressors. Rather than passive flow control methods such as vortex generator (Titchener *et al.*, 2013) and bumps (Ogawa *et al.*, 2008), the current study focus on active flow control methods. Sriram *et al.* (2014) confirmed the effectiveness of an array of tangential jets on the control of SWBLI by 20% reduction in separation length via experiments on a supersonic flow field over a wedge. White *et al.* (2015) performed both experiments and simulations to investigate the impacting parameters of the tangential mass addition under Mach number of between 3.5 and 5.0. It was claimed that the functioning jet location varies with the inlet Mach number. Under subsonic flow conditions with large scale separations and strong unsteadiness, the pulsed blowing (Hecklau *et al.*, 2011) or pulsed bleeding (Zhang *et al.*, 2018) have been reported to be more effective in the management of the flow separations and aerodynamic losses reduction. Similarly, spark jet

(Yang *et al.*, 2016) and pulsed plasma jet (Narayanaswamy *et al.*, 2012) were applied for the control of the SWBLI features. Reduction of overall magnitude of the pressure fluctuation in the low frequency band and enhanced resistance to the boundary layer separation by strengthening the mixing inside the boundary layer were observed in these studies.

In the current study, a two dimensional supersonic compressor cascade (Tweedt *et al.*, 1988) is discussed. Reynolds Averaged Navier-Stokes (RANS) equations are firstly used to acquire appropriate parameters of the excitation jet. Next, Large Eddy Simulation (LES) is performed to identify the unsteady behavior of the original flow filed without excitation. Based on the former analysis, pulsed jet is finally applied to control the SWBLI and recover the total pressure loss. Particularly, the working principle of the pulsed jet over steady excitation jet is discussed in detail.

## 2. NUMERICAL METHOD AND VALIDATION

Geometrical and aerodynamic parameters of the SL19 cascade are presented in Table 1. The current computational domain is discretized by a structured mesh and the detailed mesh distributions around the leading edge and trailing edge have been shown in Fig. 1. The mesh is refined near the walls with a standard of  $y^+$  number to be less than 1 and the streamwise and the pitchwise mesh nodes are also controlled to be fine thus the  $x^+$  number meets the requirements of LES (Gourdain, 2015). Meanwhile the mesh grid size in the streamwise is refined to ensure a better capture of the SWBLI features.

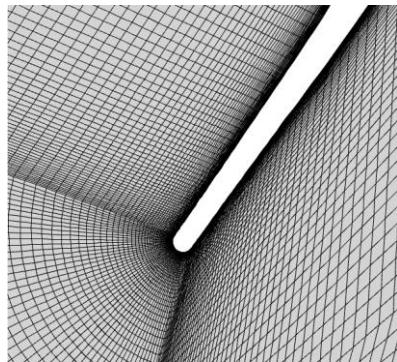
**Table 1 Geometrical and aerodynamic parameters of SL19 cascade**

parameter	value
axial chord ( $b_x$ or $c$ )	170mm
inflow $Ma$	1.45
pitch ( $t$ )	110.5mm
metal angle	148.1°
Reynolds number ( $Re$ )	$2.5 \times 10^6$

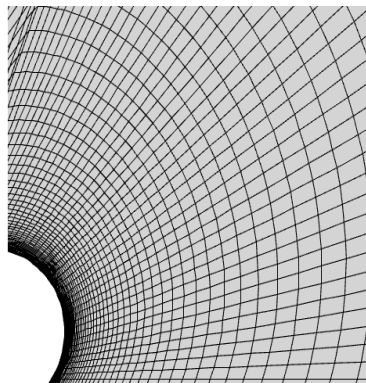
It has been validated that two dimensional LES benefits the understanding of supersonic flows and interesting conclusions has already been acquired (Venturelli *et al.*, 2016; Roohi *et al.*, 2013). The energetic larger scale motions are resolved directly and only smaller scale fluctuations are modeled under LES calculations. Thus the LES results could reserve more details of flow field fluctuations compared with unsteady Reynolds averaged Navier-Stokes equations (URANS) (Gourdain, 2015).

In the current study, calculations are accomplished under ANSYS Fluent. A steady RANS result is primarily solved as an initial flow field for LES calculations. The RANS calculation employs Shear Stress Transport  $k-\omega$  turbulent model. As for LES calculations, the central difference finite volume pressure-based solver is utilized to solve the

momentum equations with the second-order implicit format for temporal discretization and second-order up-wind format for other quantities. The second-order upwind scheme with accurate TVD techniques is employed because it provides stability for supersonic flows with reasonable stability and capture shocks with higher resolution. The dynamic kinetic energy subgrid-scale model is recommended by *ANSYS Fluent* that it is beneficial with supersonic flows so that it is used in the current study to quantify the unresolved terms. The inlet boundary conditions are set by total pressure and outlet boundary condition is presented by static pressure. Inlet turbulent intensity is given by spectral method and the non-slip adiabatic walls are implied. Appropriate times step number and Courant number are managed to ensure most velocity residual to be less than  $10^{-6}$ . The analyzed results are collected after 100 periods in the case of time duration of main flow passing the compressor cascade to be defined as one period.



(a) details at leading edge



(b) details at trailing edge

**Fig. 1. Mesh nodes distribution of SL19 cascade.**

To validate the numerical method, the time-averaged surface isentropic Mach number results of LES associated with the experimental results from literature (Tweedt *et al.*, 1988) and URANS results from literature (Venturelli *et al.*, 2016) are shown in Fig. 2. The SWBLI occurs at the  $x/c=0.65$  on the suction surface with a rapid surface isentropic Mach number drop. It should be pointed out that dual peaks that occurred in the experimental results upstream of the SWBLI region is captured in the

LES results while URANS results didn't capture.

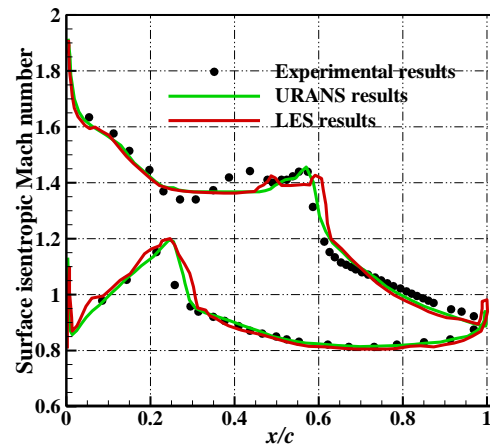


**Fig. 2. Results comparison of isentropic Mach number on blade surface.**

### 3. RESULTS AND DISCUSSION

The total pressure loss coefficient  $\omega$  is defined as shown in Eq. (1).

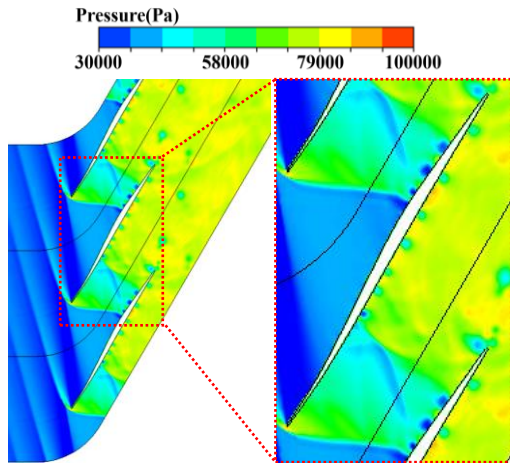
$$\omega = \frac{m_{in} \cdot p_{in}^* + m_{jet} \cdot p_{jet}^* + (m_{in} + m_{jet}) \cdot p_{out}^*}{m_{in} \cdot (p_{in}^* - p_{in}) + m_{jet} \cdot (p_{jet}^* - p_{jet})} \quad (1)$$

In Eq. (1),  $m_{in}$ ,  $p_{in}^*$ ,  $p_{in}$ ,  $m_{jet}$ ,  $p_{jet}^*$ ,  $p_{jet}$  and  $p_{out}^*$  stand for the inflow mass flow rate, inflow total pressure, inflow static pressure, jet mass flow rate, jet total pressure, jet static pressure, outflow total pressure, respectively. It should be pointed out that the total pressure loss coefficient has taken the input energy of the excitation jet into consideration.

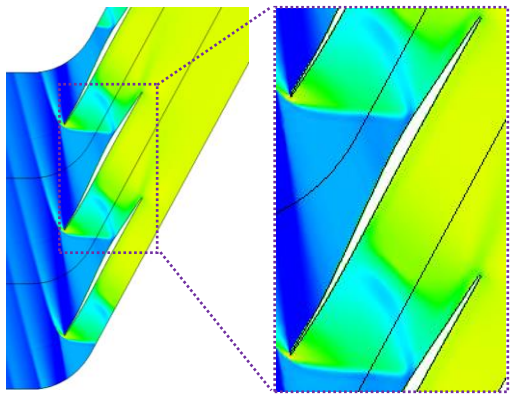
#### 3.1 Basic Features in the Original Flow Field

The flow field without excitation has been primarily simulated with LES. Figure 3(a) gives the transient absolute static pressure distribution at  $t=0.05s$ . It could be observed that strong flow field fluctuations appear mainly in three regions: the boundary layer region, the wake region and the interaction region between the shock waves and the boundary layer. Figure 3(b) presents the time-averaged absolute static pressure distribution over a period and the pressure ratio establishment of the pre-compressed profile could be explained. Two legs of the detached shock wave formulate from the blade leading edge. One of the legs forms the extended shock wave upstream of the blade and the other leg propagates into the compressor cascade and forms an oblique shock. The streams enter the compressor cascade to be decelerated and supercharged by the extended shock wave. Then, they pass a series of expansion wave and are reaccelerated and then go through the first passage oblique shock wave to be decelerated and supercharged. Finally, the streams would be reaccelerated in the passage and decelerated to be subsonic by the normal shock wave. With such shock wave distribution, the streams entering the compressor passage would be

supercharged with a pressure ratio more than 2.



(a) pressure distribution at  $t=0.05s$



(b) time-averaged pressure distribution

**Fig. 3. Pressure distribution in SL19 cascade.**

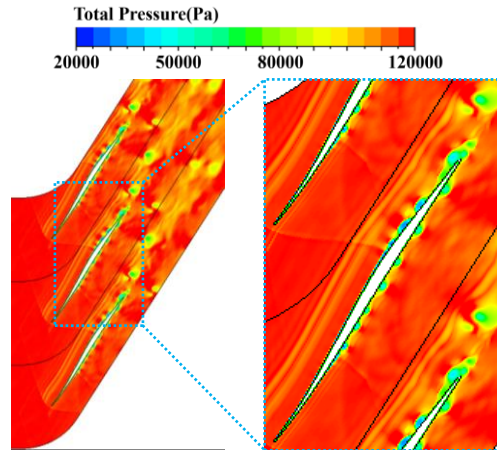
The total pressure contour helps to understand the stator losses distribution. Figure 4(a) shows the transient total pressure at  $t=0.05s$ . Some textures in a strip pattern are inferred to be the shear layer by Tweedt *et al.* (1988). There are lots of low-energy vortices in the compressor passage, especially in the wake region. Figure 4(b) presents the time-averaged total pressure distribution in the passage. The total pressure losses has two main sources (Bölcs *et al.*, 1986): one is the losses of SWBLI and shock wave losses, the other is the losses originated from the shear layer friction. It could be observed that the low total pressure particles formulate after both the oblique shock wave suction side boundary layer interaction and oblique shock wave pressure side boundary layer interaction.

### 3.2 Frequency Features in the Original Flow Field

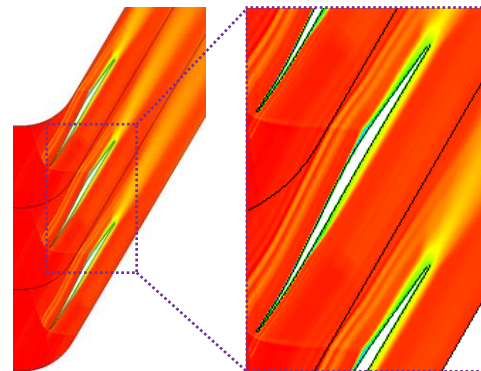
So as to take an insight to the unsteady behaviors of the original flow field, the frequency spectrums are provided in this section at different monitoring points in the flow field and under different modes of POD reconstructed flow fields. The monitoring points distribution are shown in Fig. 5, where the 1<sup>st</sup> monitoring point locates near the SWBLI region

and the 2<sup>nd</sup> to 4<sup>th</sup> points locate in the wake with  $0.13b_x$ ,  $0.42b_x$ , and  $1.00b_x$  from the blade trailing edge, respectively. Meanwhile, the Strouhal Number ( $St$ ) is utilized in the study to nondimensionalize the frequencies as Eq. (2).

$$St = \frac{b_x \cdot f}{v} \quad (2)$$



(a) total pressure distribution at  $t=0.05s$



(b) time-averaged total pressure distribution

**Fig. 4. Total pressure distribution in SL19 cascade.**

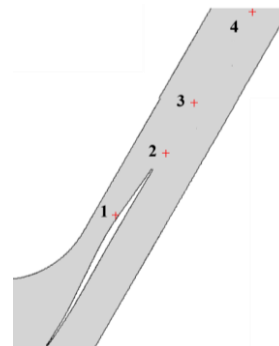


**Fig. 5. Monitoring points distribution in the flow field.**

Figure 6(a) presents the frequency spectrum of monitoring point 1 in the SWBLI region. The low frequency signals are pointed out to correspond to

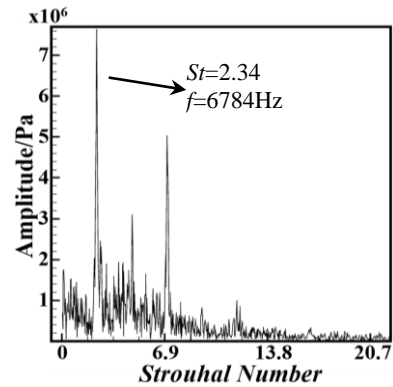
the unsteadiness of the shock wave reflection point by Pirozzoli *et al.* (2006). Consequently, the separation induced by the SWBLI would change its position rather than keep still at a fixed location. Several frequencies stand out in the frequency spectrum and  $St=2.34$  ( $f=6784\text{Hz}$ ) takes the dominating position. The power spectrum density (PSD) figure of Fig. 6(b) has several peak values in the low-frequency zone and shows an exponential decrease distribution in the high-frequency zone. The interaction of coherent structures in the boundary layer with the incident shock causes a motion of the separation bubble. Accordingly, the reflected shock fluctuates with the motion of the reflecting foot. Figure 6(c) shows the frequency spectrum at monitoring point in the wake region. The low frequency signals dominate the frequency spectrum. However, no frequency stands out compared with the case in the SWBLI region. The mixing of the vortices from both the pressure side and the suction side and the dissipation of the high frequency signals result in the low frequency distribution.

The frequency spectrums under the reconstructed flow field of POD 2<sup>nd</sup> and 3<sup>rd</sup> mode are shown in Fig. 7.  $St=2.29$  ( $f=6634\text{Hz}$ ) stands out to be the peak value in both the second mode and the third mode.

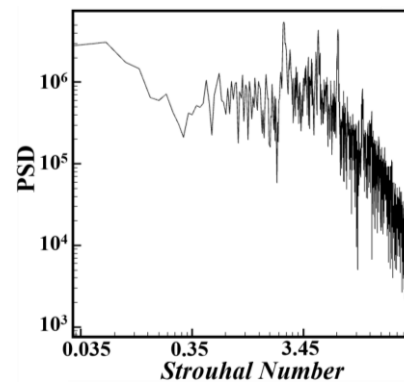
### 3.3 Performance of the Steady Excitation Jet Schemes under RANS Calculations

In order to investigate the effect of pulsed jet on the supersonic compressor cascade and to find out appropriate parameters for the pulsed jet scheme, the flow behavior under different parameters is primarily simulated with Reynolds Averaged Navier-Stokes (RANS) method under steady excitation jet conditions. The mesh grids near the excitation hole walls are refined to ensure the  $y^+$  less than 1 and the mesh grids near the excitation hole in the passage are also refined for a sufficient capture of the impact of the excitation jets on the supersonic flows. The former researches (Sriram *et al.*, 2014; Yang *et al.*, 2016; Narayanaswamy *et al.*, 2012) suggested that the excitation jet hole width  $d_{jet}$ , the excitation jet hole streamwise location  $x_{jet}$ , the excitation jet flow rate  $m_{jet}$  and the angle between excitation jet flow direction to the local surface tangent direction  $\alpha_{jet}$  are the main impacting factors of the excitation effect and gave the possible appropriate variable ranges of these parameters. Accordingly, these parameters are simulated under the variable controlling method. The total pressure loss coefficient results are shown in Table 2. Particularly, the excitation jet hole streamwise location has been non-dimensionalized. The jet hole width  $d_{jet}$  is controlled with the consideration of manufacturing demands. In addition, the excitation jet flow rate  $m_{jet}$  is chosen with management of the excitation jet velocity to be subsonic and the  $x_{jet}$  is managed to be near the SWBLI region or behind the SWBLI region. The  $\alpha_{jet}$  is set with a balance between the demand of a larger excitation jet flow rate (larger  $\alpha_{jet}$ ) and the demand of the similar jet

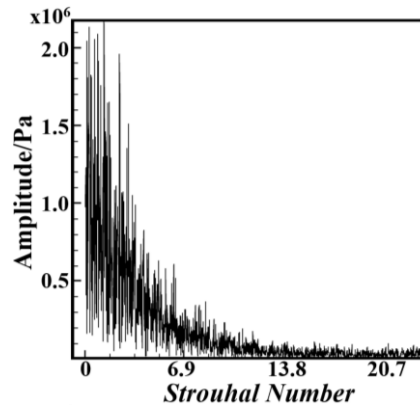
direction with the local main stream (smaller  $\alpha_{jet}$ ).



(a) frequency spectrum at point 1



(b) power spectrum density at point 1



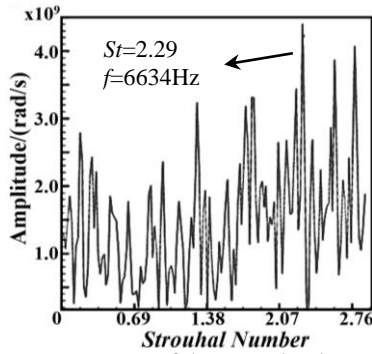
(c) frequency spectrum at point 3

**Fig. 6. Monitoring point frequency features.**

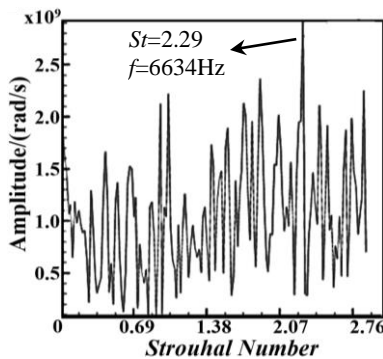
It is noticed that under the jet hole width  $d_{jet}=2.1\text{mm}$  schemes, the total pressure loss coefficient is larger than the original scheme without excitation. Considering the jet hole width  $d_{jet}=3.5\text{mm}$  schemes,  $x_{jet}=0.65$  scheme achieves better performance than other jet hole streamwise relative location in total pressure loss coefficient reduction. This suggests that the flow control application around the SWBLI position contributes to the current supersonic compressor cascade performance, which is consistent with the conclusion of former researches (Sriram *et al.*, 2014; Narayanaswamy *et al.*, 2012).

**Table 2 Total pressure loss coefficient under different cases**

Cases under different $x_{jet}$ ( $m_{jet}=0.072\text{kg/s}$ , $\alpha_{jet}=64^\circ$ , $d_{jet}=2.1\text{mm}$ )				Cases under different $x_{jet}$ ( $m_{jet}=0.072\text{kg/s}$ , $\alpha_{jet}=64^\circ$ , $d_{jet}=3.5\text{mm}$ )				without excitation
$x_{jet}$	0.65	0.75	0.85	$x_{jet}$	0.65	0.75	0.85	
$\omega$	0.09608	0.09715	0.09720	$\omega$	0.08748	0.09480	0.09500	0.09546
Cases under different $\alpha_{jet}$ ( $m_{jet}=0.072\text{kg/s}$ , $d_{jet}=2.1\text{mm}$ , $x_{jet}=0.65$ )				Cases under different $m_{jet}$ ( $\alpha_{jet}=64^\circ$ , $d_{jet}=2.1\text{mm}$ , $x_{jet}=0.65$ )				
$\alpha_{jet}$	64	64.5	65.5	$m_{jet}$	0.035	0.052	0.065	0.072
$\omega$	0.08748	0.08767	0.08798	$\omega$	0.0980	0.09620	0.09380	0.08748



(a) frequency spectrum of the second order mode



(b) frequency spectrum of the third order mode

**Fig. 7. Frequency spectrum at different modes of POD reconstructed flow field.**

### 3.4 Performance of the Pulsed and Steady Excitation Jet Schemes under LES

It is concluded from the former sections that the flow field in the supersonic compressor cascade is accompanied with strong unsteady behaviors. As a result, the discussion of the pulsed excitation jet on the control effects of the SWBLI features and the recovery of the total pressure losses could be valuable. In consideration of the results of the governing parameters in Section 3.3, the jet hole width, location and direction are chosen to be  $d_{jet}=3.5\text{mm}$ ,  $x_{jet}=0.65$  and  $\alpha_{jet}=64^\circ$ , respectively. Figure 8 gives the unsteady calculation cases under LES with one pulsed excitation jet scheme and two comparison schemes under steady excitation jet. The mean flow rate of the pulsed excitation jet scheme is chosen to be  $0.035\text{kg/s}$  to avoid supersonic flow conditions during the whole excitation period. Similar frequencies have been

observed with the frequency at the monitoring point near the SWBLI region and the frequency of the second and third mode of the POD reconstructed flow field in section 3.2. Accordingly, the pulsed excitation frequency is chosen to be  $6700\text{Hz}$  ( $St=2.31$ ).

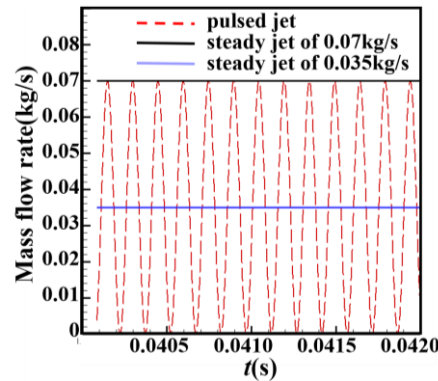
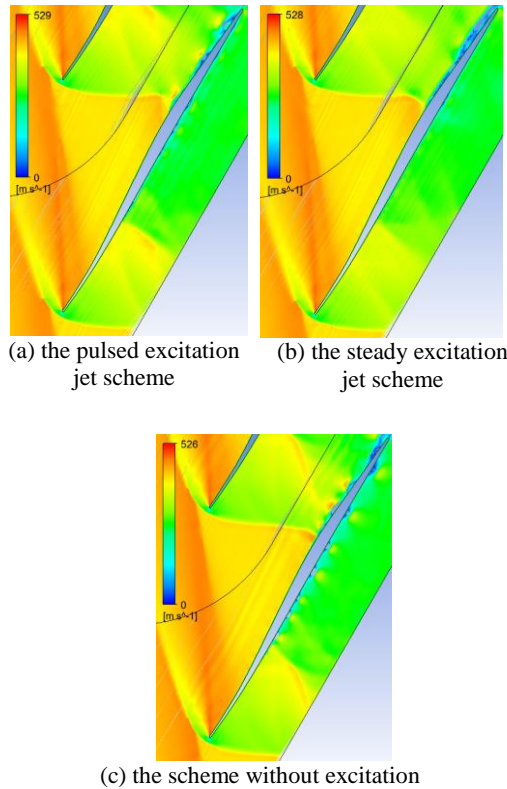


**Fig. 8. Excitation jet mass flow rate distribution of different cases.**

The period of the pulsed excitation jet scheme is defined as  $1/f=0.00015\text{s}$  and the time-averaged results are collected over 200 periods. The pulsed excitation jet scheme and the steady excitation jet with  $m_{jet}=0.035\text{kg/s}$  scheme share the same excitation jet mass flow rate, while the former scheme achieves a total pressure loss coefficient of  $\omega=0.0884$ , 9.8% reduction compared with the latter scheme. Besides, the steady excitation jet with  $m_{jet}=0.07\text{kg/s}$  scheme acquires two times the mass flow rate of the pulsed excitation jet scheme and it achieves a total pressure loss coefficient of  $\omega=0.0884$ , 10.3% reduction compared with the original case without excitation. Figure 9 presents the transient velocity contour near the profile under different schemes. It is observed from Fig. 9(c) that several vortices appear on the suction surface behind the oblique shock wave suction surface boundary layer interaction region and on the pressure surface behind the reflection shock wave pressure surface boundary layer interaction region. These vortices have been suppressed in the schemes with excitation jets. It is pointed out that the excitation jets arranged on the suction surface not only impact the SWBLI on the suction surface, but also impact that on the pressure surface via the management of the reflection shock wave.



(a) the pulsed excitation jet scheme (b) the steady excitation jet scheme

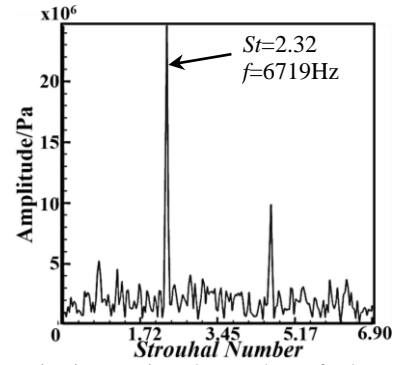
(c) the scheme without excitation

**Fig. 9. Transient velocity contour at  $t=0.05s$  in the compressor cascade.**

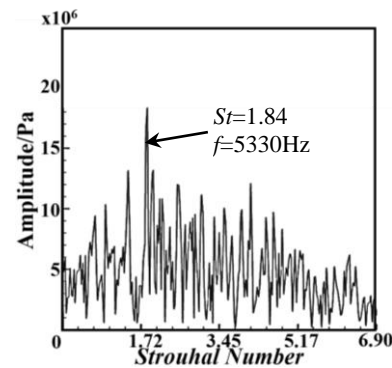
### 3.5 The Frequency Features of the Schemes under LES

With a purpose of better understanding to the unsteadiness in the flow field, the frequency spectrums of total pressure at several monitoring points of different axial locations are shown in Fig. 10. The monitoring points distribution in the flow field could be found in Fig. 5.

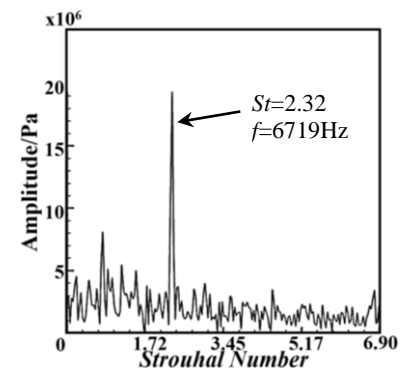
The results in Figs. 10(a), (c) and (e) present the frequency spectrums of the pulsed excitation jet scheme at different axial locations. A dominating frequency of  $f=6719$  Hz ( $St=2.32$ ) is identified among all the three results, corresponding to the excitation frequency of  $f=6700$  Hz ( $St=2.31$ ). Thus it can be inferred that the excitation frequency dominates the flow field in both the regions near the excitation jet area and the regions away from the excitation jet. Meanwhile, it is noticed that the high frequencies tend to fade in the frequency spectrums as the fluids flow downstream in the cascade. This tendency reveals the trend of the high frequency dissipation in the flow field and the transformation of the vortices frequencies towards low frequencies. Besides, the dominating frequencies of the steady excitation jet scheme at monitoring point 2, 3 and 4 are  $f=5330$  Hz ( $St=1.84$ ),  $f=2740$  Hz ( $St=0.94$ ) and  $f=1935$  Hz ( $St=0.67$ ), respectively. The frequencies distributions are more uniform compared with the pulsed excitation jet scheme. The similar dissipation of the high frequencies and similar transformation of the vortices frequencies towards low frequencies are observed between the two schemes.



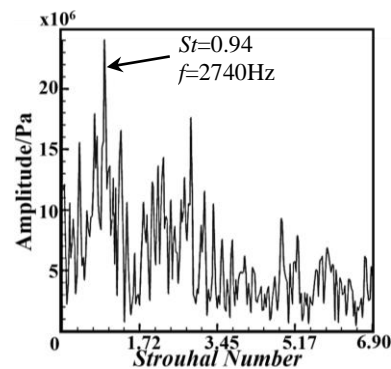
(a) monitoring point 2 results of the pulsed excitation jet scheme



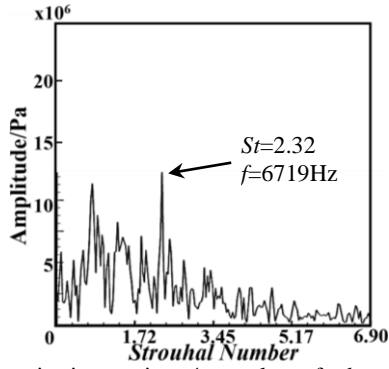
(b) monitoring point 2 results of the steady excitation jet scheme



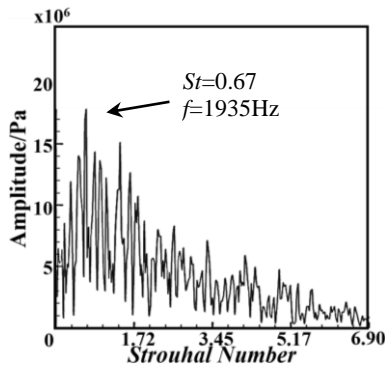
(c) monitoring point 3 results of the pulsed excitation jet scheme



(d) monitoring point 3 results of the steady excitation jet scheme



(e) monitoring point 4 results of the pulsed excitation jet scheme



(f) monitoring point 4 results of the steady excitation jet scheme

**Fig. 10. Frequency spectrum at different locations and different excitation schemes.**

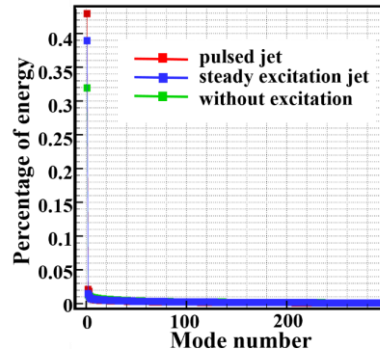
### 3.6 POD Analysis of the Schemes

The Proper Orthogonal Decomposition (POD) analysis of the LES results are performed in the current section to take an insight to the unsteadiness information of the supersonic flow field. Plural velocity can reflect the kinetic energy and compression information in the flow field and is defined as Eq. (3). It should be noted that time-averaged flow field information is retained in the current POD analysis.

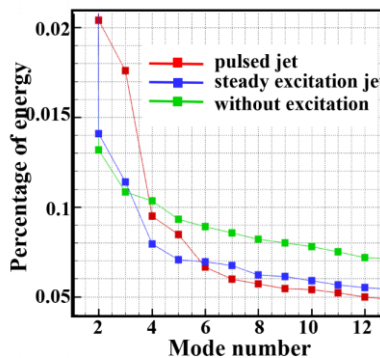
$$v_{plural} = \sqrt{\rho}(u + vi) \quad (3)$$

Figure 11 presents the kinetic energy percentage distribution with different mode numbers under different schemes. The first mode stands for the time-averaged flow field and the other modes stand for the fluctuation information in the flow field. It is observed that the first mode dominates most energy in the flow field and the energy percentage decreases dramatically with the increase of the mode number. In addition, it is noticed that both the steady excitation jet and the pulsed jet gather the energy to the low orders of the modes, especially the first four modes. It could be concluded that the pulsed excitation jet converts more energy to the low modes compared with the steady excitation jet scheme. The lower POD modes usually represent the large-scale coherent structures in the boundary layer that

dominate the global flow field and occupy most of energy. Thus converting more energy to the low modes lead to a reduction in the flow structure coherence (Arunajatesan, 2009)



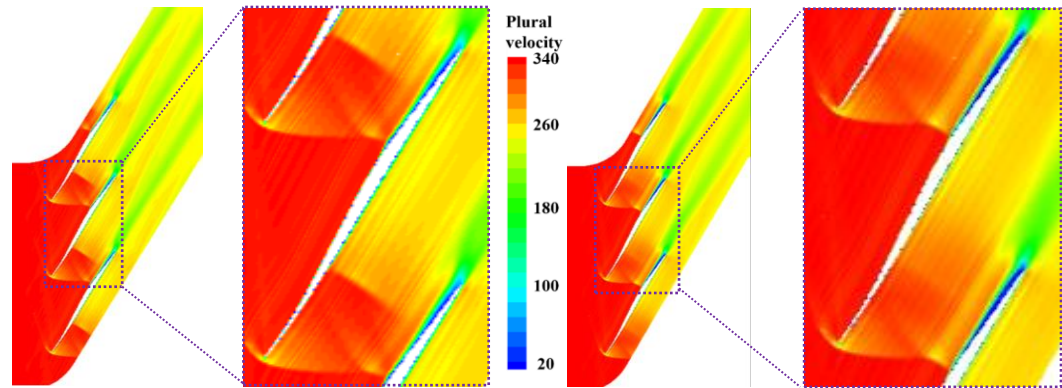
(a) energy percentage distribution of the first 300 modes



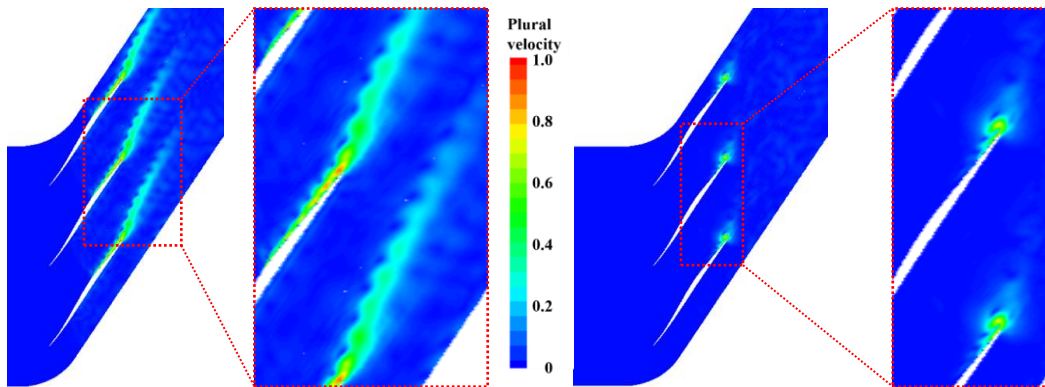
(b) energy percentage distribution of 2nd to 12th modes

**Fig. 11. Energy percentage distribution of different schemes.**

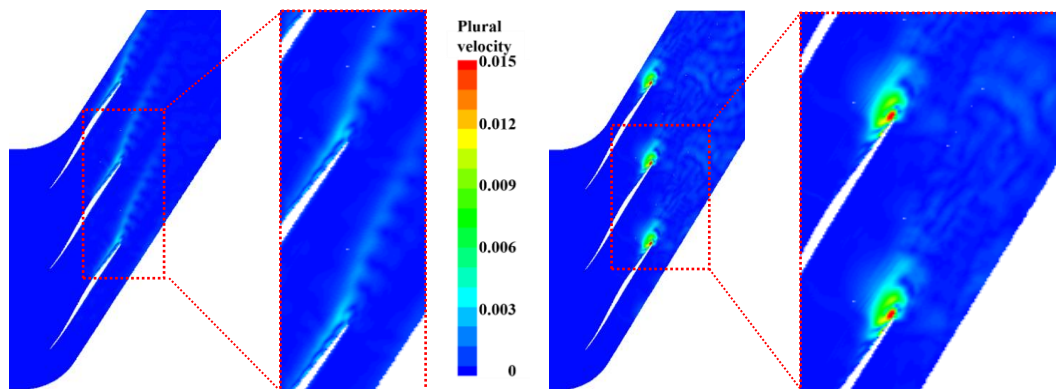
The reconstructed first three modes plural velocity contours under different schemes are shown in Fig. 12. The shock wave structures can be identified with the first mode of the plural velocity contours in Figs. 12(a) and (b). If determine the normal shock wave strength by the static pressure ratio before and after the shock wave, it would be observed that the normal shock wave in the passage of the pulsed excitation jet scheme is stronger than that in the passage of the steady excitation jet scheme. These results match the result in Fig. 9. The plural velocity contours of the second and third order modes under the pulsed excitation jet scheme indicate that the functioning area of the pulsed excitation jet concentrate on the SWBLI region and its downstream region with obvious fluctuations. With the help of the frequency spectrums in Fig. 10, the dominating frequency in the functioning regions is consistent with the excitation frequency. However, the plural velocity contours of the second and third order modes under the steady excitation jet scheme show no obvious fluctuation and the unsteady regions correspond to the separation flows and vortices.



(a) 1<sup>st</sup> mode plural velocity of pulsed jet scheme (left) and steady jet scheme (right)



(b) 2<sup>nd</sup> mode plural velocity of pulsed jet scheme (left) and steady jet scheme (right)



(c) 3<sup>rd</sup> mode plural velocity of pulsed jet scheme (left) and steady jet scheme (right)

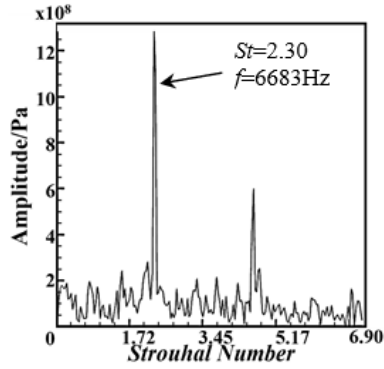
**Fig. 12. Plural velocity contour of the first three modes under different schemes.**

Figure 13 provides the time coefficient frequency spectrums under the first three modes of different excitation schemes. The pulsed excitation jet scheme results share the same peak frequency of  $f=6683$  Hz ( $St=2.30$ ), which is related to the excitation frequency of  $f=6700$  Hz ( $St=2.31$ ) and the governing frequency of  $f=6719$  Hz ( $St=2.32$ ) in Section 3.5. Such frequency spectrums indicate that the pulsed excitation jet regulates not only the time-averaged flow field, but also the second and third modes which stand for the unsteady structures in the flow field. As for the steady excitation jet scheme, several peak frequencies such as  $f=5330$  Hz ( $St=1.84$ ) and  $f=6478$  Hz ( $St=2.23$ ) stand out but no dominating frequency exists.

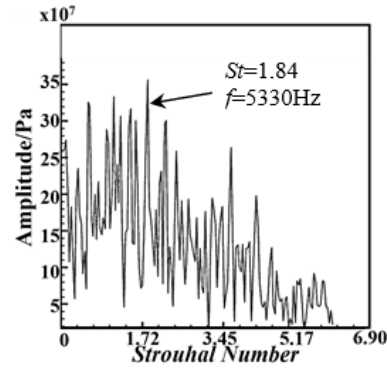
#### 4. CONCLUSION

The original flow field without excitation in a supersonic compressor cascade is analyzed in detail with LES calculations. Some governing parameters of the excitation jets are chosen based on RANS results. Regards to the results of frequency spectrum and POD analysis, the excitation jet frequency is chosen for the pulsed excitation jet scheme. Several conclusions are drawn from the results:

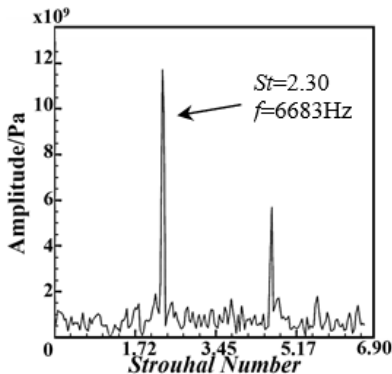
- 1) Strong flow field fluctuation occurs in the shock wave and boundary layer interaction region, which is also the main source of the total losses. Both low-frequency signals and high-frequency



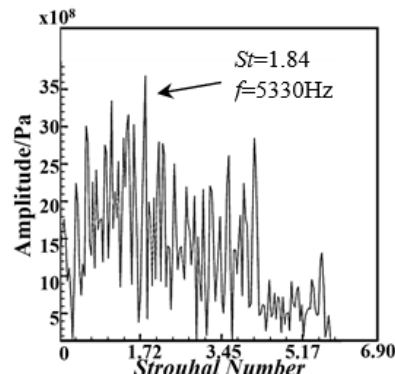
(a) 1<sup>st</sup> mode time coefficient frequency spectrum of pulsed excitation jet scheme



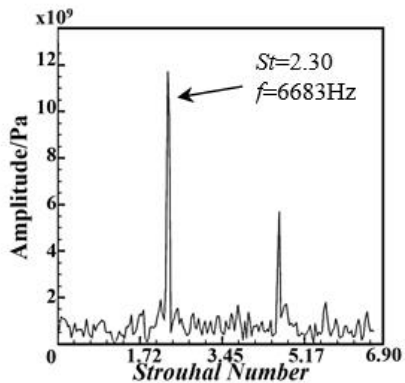
(b) 1<sup>st</sup> mode time coefficient frequency spectrum of steady excitation jet scheme



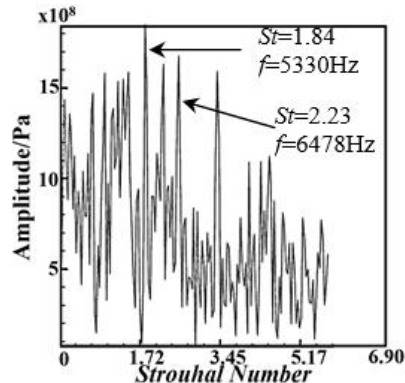
(c) 2<sup>nd</sup> mode time coefficient frequency spectrum of pulsed excitation jet scheme



(d) 2<sup>nd</sup> mode time coefficient frequency spectrum of steady excitation jet scheme



(e) 3<sup>rd</sup> mode time coefficient frequency spectrum of pulsed excitation jet scheme



(f) 3<sup>rd</sup> mode time coefficient frequency spectrum of steady excitation jet scheme

**Fig. 13. Time coefficient frequency spectrum of the first three modes under different schemes.**

signals exist in this region, while the low-frequency signals correspond to the unsteadiness of the shock wave reflection point. With the mixing effect and high dissipation rate of the high-frequency signals, the high-frequency signals shrink in the wake and the flow field builds up more uniformity.

- 2) The frequency spectrums in the SWBLI region and the second and third mode of time coefficient suggest that  $f=6700\text{Hz}$  ( $St=2.31$ ) to

be the excitation frequency of the pulsed jet scheme. As a result, a dominating frequency of  $f=6719\text{ Hz}$  ( $St=2.32$ ) in the frequency spectrums and a dominating frequency of  $f=6683\text{ Hz}$  ( $St=2.30$ ) in the time coefficient by the POD analysis in the pulsed excitation jet scheme results are identified. This infers that the excitation frequency dominates the flow field in both the regions near the excitation jet area and the regions away from the excitation jet and not only the time-averaged flow field, but also the

second and third modes which stand for the unsteady structures in the flow field.

- 3) The pulsed excitation jet scheme achieves a 9.8% reduction of total pressure loss compared with the steady excitation jet scheme under the same time-averaged excitation jet mass flow rate. The excitation jets arranged on the suction surface not only impact the boundary layer separation on the suction surface, but also impact the separation on the pressure surface via the management of the reflected shock wave.
- 4) In the POD analysis, the first mode stands for the time-averaged flow field and the other modes stand for the fluctuation information in the flow field. The first mode dominates most energy in the flow field and the energy percentage decreases dramatically with the increase of the mode number. Compared with the steady excitation jet scheme, the pulsed excitation jet scheme gathers more energy to the low orders of the modes, especially the first four modes.

#### ACKNOWLEDGEMENTS

This study is financially supported by National Natural Science Foundation of China (Grant No. 51776048 and 51436002)

#### REFERENCES

- Arunajatesan, S., C. Kannepalli, N. Sinha and M. Sheehan, F. Alvi, G. Shumway and L. Ukeiley (2009). Suppression of cavity loads using leading-edge blowing. *AIAA journal* 47(5), 1132-1144.
- Biollo, R. and E. Benini (2013). Recent advances in transonic axial compressor aerodynamics. *Progress in Aerospace Sciences* 56(1), 1-18.
- Bölcs, A. and P. Suter (1986). Transsonische Turbomachinen, In *Wissenschaft und Technik: Taschenausgabe*, G. Braun, Karlsruhe.
- Calvert, W. and A. Stapleton (1994). Detailed flow measurements and predictions for a three-stage transonic fan. *Journal of Turbomachinery* 116(2), 298-305.
- Chauvin, J., C. Sieverding and H. Griepentrog (1969). Flow in cascade with transonic regime. *Proceeding of Symposium of Flow Research on Blading* 151-196.
- Cizmas, A., G. Paul and A. Palacios (2003). Proper orthogonal decomposition of turbine rotor-stator interaction. *Journal of Propulsion and Power*, 19(2), 268-281.
- Clemens, N. and V. Narayanaswamy (2014). Low-frequency unsteadiness of shock wave turbulent boundary layer interactions. *Annual Review of Fluid Mechanics* 46, 469-492.
- Gourdain, N. (2015). Prediction of the unsteady turbulent flow in an axial compressor stage. Part 1: Comparison of unsteady RANS and LES with experiments. *Computers & Fluids* 106, 119-129.
- Griepentrog, H. (1972). Shock wave boundary layer interaction in cascades. *Agardograph Na 164 on Boundary Layer Effects in Turbo Machines*, 1972, 443-456.
- Hecklau, M., O. Wiederhold, V. Zander, R. King, W. Nitsche and A. Huppertz (2011). Active separation control with pulsed jets in a critically loaded compressor cascade. *AIAA journal* 49(8), 1729-1739.
- Horstman, C., G. Settles, I. Vas, S. Bogdonoff and C. Hung (1977). Reynolds Number Effects on Shock-Wave Turbulent Boundary-Layer Interactions. *AIAA Journal* 15(8), 1152-1158.
- Humble, R., G. Elsinga and B. Oudheusden (2009, June). Time series analysis of a shock wave/turbulent boundary layer interaction using a dynamical systems approach. In *39th AIAA Fluid Dynamics Conference*. San Antonio, Texas, Paper No.3713.
- Kuacute, B. and H. Schreiber (1998). Compressor cascade flow with strong shock wave/boundary layer interaction. *AIAA Journal* 36(11), 2072-2078.
- Liepmann, H. W., A. Roshko and S. Dhawan (1951). On reflection of shock waves from boundary layers. In *California Institute of Technology*, Report No. TN 2334.
- Liu, B., H. Shi and X. Yu (2017). A new method for rapid shock loss evaluation and reduction for the optimization design of a supersonic compressor cascade. *Proceedings of the Institution of Mechanical Engineers, Part G: Journal of Aerospace Engineering* 232(13), 2458-2476.
- Lumley, J., A. Yaglom and V. Tatarski (1967). Atmospheric turbulence and radio wave propagation. *Journal of Computational Chemistry* 23(13), 1236-1243.
- Narayanaswamy, V., L. Raja and N. Clemens (2012). Control of unsteadiness of a shock wave turbulent boundary layer interaction by using a pulsed plasma jet actuator. *Physics of Fluids* 24(7), 076101.
- Ogawa, H., H. Babinsky, M. Pätzold and T. Lutz (2008). Shock wave boundary layer interaction control using three-dimensional bumps for transonic wings. *AIAA journal* 46(6), 1442-1452.
- Pasquariello, V., S. Hickel and N. Adams (2017). Unsteady effects of strong shock wave boundary layer interaction at high Reynolds number. *Journal of Fluid Mechanics* 823, 617-657.
- Pearcey, H. (1959). Some effects of shock-induced separation of turbulent boundary layers in

- transonic flow past airfoils. *Aeronautical Research Council Reprint and Memoranda*. Report No.3108.
- Pirozzoli, S. and F. Grasso (2006). Direct numerical simulation of impinging shock wave turbulent boundary layer interaction at  $Ma=2.25$ . *Physics of Fluids* 18(6), 065113.
- Priebe, S. and M. Martín (2012). Low-frequency unsteadiness in shock wave turbulent boundary layer interaction. *Journal of Fluid Mechanics* 699, 1-49.
- Priebe, S., M. Wu and M. Martin (2009). Direct numerical simulation of a reflected shock wave/turbulent boundary layer interaction. *AIAA Journal* 47(5), 1173-1185.
- Roohi, E., A. Zahiri and F. Passandideh (2013). Numerical simulation of cavitation around a two-dimensional hydrofoil using VOF method and LES turbulence model. *Applied Mathematical Modelling* 37(9), 6469-6488.
- Soni, R., N. Arya and A. De (2017). Characterization of turbulent supersonic flow over a backward-facing step. *AIAA Journal* 55(5), 1-19.
- Sriram, R. and G. Jagadeesh (2014). Shock tunnel experiments on control of shock induced large separation bubble using boundary layer bleed. *Aerospace Science and Technology* 36, 87-93.
- Titchener, N. and H. Babinsky (2013). Shock wave boundary layer interaction control using a combination of vortex generators and bleed. *AIAA Journal* 51(5), 1221-1233.
- Tweedt, D., H. Schreiber and H. Starcken (1988). Experimental investigation of the performance of a supersonic compressor cascade. *Journal of Turbomachinery* 110(4), 456-466.
- Vanstone, L., M. Saleem, S. Seckin and N. Clemens (2016). Effect of upstream boundary layer on unsteadiness of swept-ramp shock/boundary layer interactions at Mach 2. In *54th AIAA Aerospace Sciences Meeting*. San Diego, California, Paper No.0076.
- Venturelli, G. and E. Benini (2016). Kriging-assisted design optimization of S-shape supersonic compressor cascades. *Aerospace Science and Technology* 58, 275-297.
- White, M., R. Lee, M. Thompson, A. Carpenter and W. Yanta (2015). Tangential mass addition for shock boundary layer interaction control in scramjet inlets. *Journal of Propulsion and Power* 7(6), 1023-1029.
- Yang, G., Y. Yao, J. Fang, T. Gan, Q. Li and L. Lu (2016). Large-eddy simulation of shock wave turbulent boundary layer interaction with and without spark jet control. *Chinese Journal of Aeronautics* 29(3), 617-629.
- Zhang, H., S. Chen, Q. Meng and S. Wang (2018). Using unsteady pulsed suction through endwall bleeding holes in a highly loaded compressor cascade. *Aerospace Science and Technology* 72, 455-464.